ARTICLE IN PRESS

Available online at www.sciencedirect.com

ScienceDirect

Microporous and Mesoporous Materials xxx (2007) xxx–xxx

MICROPOROUS AND MESOPOROUS MATERIALS

www.elsevier.com/locate/micromeso

Study of the microstructure of amorphous aluminosilicate gel before and after its hydrothermal treatment

Cleo Kosanović [a,*], Sanja Bosnar [a], Boris Subotić [a], Vesna Svetličić [a], Tea Mišić [a], Goran Dražić [b], Károly Havancsák [c]

[a] *Ruđer Bošković Institute, Bijenička 54, 10000 Zagreb, Croatia*
[b] *Jožef Stefan Institute, Jamova 39, 1000 Ljubljana, Slovenia*
[c] *Eotvos Lorand University, Department of Solid State Physics, Pazmany P. s. 1/A, 1117 Budapest, Hungary*

Received 3 April 2007; received in revised form 5 June 2007; accepted 6 June 2007

Abstract

Solid phase (gel) separated from freshly prepared sodium aluminosilicate hydrogel as well as during its hydrothermal treatment at 80 °C was analyzed by different methods such as powder X-ray diffraction (XRD), Fourier transform infrared spectroscopy (FTIR), differential thermal gravimetry (DTG), high-resolution transmission electron microscopy (HRTEM) and atomic force microscopy (AFM). Analysis of the obtained results have shown that the freshly prepared gel is mainly composed of disc-shaped primary particles, but also partially or even fully crystalline entities were observed by AFM analysis. AFM analysis of the solids separated from the hydrogel at various stages of its hydrothermal treatment (heating at 80 °C) indicates that the particles of the partially and/or fully crystalline phase are nuclei for further crystallization of zeolite. Although it is assumed that the nuclei have structure of faujasite rather than zeolite A, further growth of zeolite A was readily explained by the fact that regardless of the "structure" of nuclei, the type of zeolite to be formed is determined by the concentrations of silicon and aluminum in the liquid phase of the crystallizing system.

Keywords: Aluminosilicate gel; Zeolite A; Atomic force microscopy; Microstructure; Nucleation

1. Introduction

Different types of zeolites can be obtained by heating both homogeneous (clear solutions) and heterogeneous (hydrogels) alkaline aluminosilicate precursors [1]. The type of zeolite to be crystallized depends to a large extent on the chemical composition of its precursor and the mode of its preparation, and to a lesser extent, on the crystallization conditions [1,2]. In both cases, crystallization takes place by formation of primary zeolite particles (nuclei) and their solution-mediated growth from solution supersaturated with active aluminate, silicate and aluminosilicate anions [1]. While the mechanism of the crystal growth of zeolites is well defined by the reactions of active aluminate, silicate and/or aluminosilicate species from the liquid phase on the surface of growing zeolite crystals [3] and revealed by numerous AFM studies [4–7], there is still much uncertainty regarding the relevant mechanisms of zeolite nucleation [1]. Although various nucleation mechanisms such as homogeneous [8], heterogeneous [9] and secondary nucleation [10] in the liquid phase supersaturated with soluble aluminate, silicate and aluminosilicate species as well as a nucleation process on the gel/liquid interface [11] have been proposed as the processes relevant for the formation of primary zeolite particles, there is abundant experimental evidence that due to the high supersaturation of constituents (Na, Si, Al, template) in gel [12–15], a considerable amount of nuclei are formed in the gel and/or at the gel/liquid interface by a linking of specific subunits during gel precipitation and/or ageing [15–22]. In addition,

* Corresponding author. Tel.: +385 1 45 61 184; fax: +385 1 46 80 098.
E-mail address: cleo@irb.hr (C. Kosanović).

1387-1811/$ - see front matter © 2007 Elsevier Inc. All rights reserved.
doi:10.1016/j.micromeso.2007.06.007

recent scattering studies of clear (alumino)silicate solutions have suggested that even in the homogeneous precursors zeolite nucleation does not occur in the solution phase as one might imagine from classical nucleation concepts, but that zeolite crystals nucleate in amorphous gel particles formed in the first step of the crystallization process [15,22]. Hence, it is very probable that solid amorphous phase (gel) of aluminosilicate hydrogel is not only a ''reservoir'' of active aluminate, silicate and/or aluminosilicate species needed for crystal growth, but also the source of nuclei in both homogeneous and heterogeneous aluminosilicate precursors. Because the nuclei (particles of partially crystalline or ''quasi-crystalline'' phase) [16] cannot grow, or their growth is considerably retarded due to the slow transport of material inside the gel matrix [23], they are potential nuclei when they are ''hidden'' in the gel matrix, and can start to grow after their ''release'' from the gel dissolved during the crystallization, i.e., when they are in full contact with the liquid phase (autocatalytic nucleation) [24–27].

The observation that nuclei cannot grow (or that their growth is considerably retarded) in the gel matrix is in contrast with recent observation that small, nano-sized crystals of zeolites A and X formed in the gel matrix, grow inside the gel particles [15,22]. This is argued by both the HRTEM pictures of the solid phase at different stages of room-temperature ageing and hydrothermal treatment as well as by the fact that ''The amorphous gel-zeolite particles maintained their average size over the course of complete conversion into (more dense) zeolite A, suggesting that mass transfer from solution supplies some of precursor material''. However, it must be noted that in these cases the amorphous phase was formed as discrete particles, having 40–80 nm in size, during room-temperature ageing of diluted, initially clear aluminosilicate solution. Hence, it is quite possible that density of these amorphous particles is low enough for ''free'' transport of material through the gel–solution interface as well as inside the gel matrix. On the other hand, it is really to assume that due the high aluminosilicate concentration, the primary gel particles formed from heterogeneous systems have higher density than those formed from homogeneous systems (clear solutions); these primary gel particles have a strong tendency to form dense packed agglomerates having the size in the micrometer range [24,28–32] (see also Figs. 4 and 6 in this work). Under such conditions the transport of material through the gel–solution interface is limited to thin surface/subsurface layers of gel particles. This is possible reason that nuclei are concentrated in the surface/subsurface layer of the gel particles [33] and that their concentration decreases towards the nutrients of the gel particles [34]. Hence, it is clear that crystallization starts by the growth of nuclei positioned at the surface of gel particles and continues by the growth of the nuclei released from the gel dissolved in the further course of the crystallization process. Such occurrence of the crystallization process (autocatalytic nucleation) can be clearly argued by the existence of distinctly separated growing zeolite crystals and dissolving gel particles during the entire process of crystallization [24,28–32] in spite of maintaining the gel-zeolite particle size in an assumed growth inside gel matrix [15,22].

Analysis of the kinetics of many crystallizations of different types of zeolites revealed the idea of autocatalytic nucleation [19,24–27,33,35]. The presence of long-range ordered (partially crystallized, ''quasi-crystalline'') phase, comparable with zeolite structure (potential nuclei) in amorphous aluminosilicates (gels) was assumed and/or indirectly detected by using different experimental techniques such as ^{27}Al NMR [36,37], ^{29}Si NMR [37], ^{13}C NMR [37], differential thermal analysis [18,19,37], diffuse reflectance [38] and electron diffraction [19,39]. However, the results of direct microscopic (HRTEM) observation of the long-range ordered (''quasi-crystalline'') phase in the gel matrix [16,40] or even nano-sized zeolite crystals embedded in the gel particles [15,22], appeared in only few papers [15,16,22,40]. Hence, the questions – what is the real size of zeolite nuclei and what do the zeolite nuclei look like – are still in the domain of speculation. On the other hand, recent AFM studies of different types of zeolites [4–7,41–46] have shown that this method enables direct observation of the structural and morphological entities of zeolite crystals (e.g., growing terraces whose thickness is closely related to structure, small pyramidal structures related to surface nuclei, double 4-rings on zeolite LTA crystal surface and 12-membered rings on the (0 0 1) surface of mordenite crystals) that cannot be observed by other methods. The success in the AFM studies of zeolites offers new possibilities in the study of surface and micro-structural particularities of the amorphous aluminosilicate precursors of zeolite crystallization.

Hence, the objective of this work is to investigate micro-structural particularities of the amorphous aluminosilicate precursor and their changes during hydrothermal treatment (crystallization of zeolite) using AFM as the main experimental method and other techniques such HRTEM, XRD, FTIR and DTG as additional (auxiliary) experimental methods. To our knowledge, micro-structural properties of amorphous aluminosilicate precursor and their changes at the earliest stage of the crystallization process has not been studied by AFM technique.

2. Experimental

2.1. Samples preparation

Aluminosilicate hydrogel having the molar batch composition $3.51Na_2O \cdot Al_2O_3 \cdot 2.15SiO_2 \cdot 85.20H_2O$ was prepared by rapid addition (in 10 s) of 150 ml of Na-silicate solution (1.297 mol dm^{-3} in SiO_2 and 1.365 mol dm^{-3} in Na_2O) into a plastic vessel contained 150 ml of stirred (by propeller) Na-aluminate solution (0.603 mol dm^{-3} in Al_2O_3 and 0.754 mol dm^{-3} in Na_2O). Sodium silicate solution was prepared by dissolution of fumed silica in NaOH solution. Sodium aluminate solution was prepared by dis-

solution of aluminum wire in NaOH solution. A part of the hydrogel was centrifuged to separate the solid amorphous phase from the liquid phase (supernatant). After removal of the supernatant, the solid phase was redispersed in demineralized water and centrifuged repeatedly. The procedure was repeated until the pH value of the liquid phase above the sediment was 9. The wet washed solids were dried overnight at 105 °C and cooled in a desiccator over silicagel. The rest of hydrogel was heated at 80 °C and aliquots of the reaction mixture were drawn off at different crystallization times t_c (= 10, 30, 90 and 240 min after beginning of heating). The aliquots were poured into cuvettes and were centrifuged to stop the crystallization process and to separate the solid from the liquid phase. After removal of the supernatant, the solid phase was redispersed in distilled water and centrifuged repeatedly. The procedure was repeated until the pH value of the liquid phase above the sediment was about 9. The wet washed solids were dried overnight at 105 °C, and cooled in a desiccator over silicagel. The solid samples prepared as described above were analyzed/characterized by the following techniques.

2.2. Sample analysis/characterization

2.2.1. X-ray powder diffraction (XRD)

The X-ray diffraction patterns of the samples were taken by a Philips PW 1820 diffractometer with vertical goniometer and Cu Kα graphite radiation.

2.2.2. Fourier transform infrared spectroscopy (FTIR)

Infrared transmission spectra of the samples were made by the KBr wafer technique. The spectra were recorded on an FTIR. Spectrometer System 2000 FT-IR (Perkin–Elmer).

2.2.3. Thermal analysis

Thermogravimetric (TGA) and differential thermogravimetric (DTG) analysis, respectively, of gels was performed on a SDT 2960 thermal analysis system (TA Instruments, Inc.). The measurements were carried out in nitrogen flow with a heating rate of 10 °C/min.

2.2.4. Chemical composition

The chemical composition of the gel (contents of Na, Al, Si) was determined using EDXS and thermal analysis (H_2O content).

2.2.5. High-resolution transmission electron microscopy (HRTEM)

A powdered sample was mixed with ethanol and a drop of suspension was placed on a lacy carbon-coated Cu grid. Samples were examined by a JEOL 2010F transmission electron microscope equipped with a field emission gun and operated at 200 kV. Energy dispersive X-ray spectroscopy (LINK ISIS-300, with an UTW Si–Li detector) was employed for chemical composition determination. HRTEM images and the selected area electron diffraction (SAED) method were used for determining the crystallinity of samples.

2.2.6. Atomic force microscopy (AFM)

The powdered sample was suspended in ultra-pure water (1 g/L) and stirred for 1 h. The suspension was diluted in ultra-pure water so that the final suspension contained 10 mg of powder/L. Five liter of the final suspension were pipetted directly onto freshly cleaved mica. Following deposition, the mica sheets were placed in enclosed Petri dishes for several hours at a relative humidity of 50% in order to evaporate the excess of water. AFM imaging was performed using Multimode Scanning Probe Microscope with Nanoscope IIIa controller (Veeco Instruments, Santa Barbara, CA) with a vertical engagement (JV) 125 μm scanner. Images were collected using mainly tapping mode AFM because it is particularly well adapted to soft samples due to a nearly complete reduction of lateral forces. "Light tapping" was applied using silicon tips (TESP, Veeco) and silicon nitride (NP-20, Veeco) for contact mode. While imaging in contact mode the minimum force to maintain contact between the probe and the scanned surface was used. AFM of the sample obtained after 90 min of hydrothermal treatment was performed in air using a Solver PRO scanning probe microscope (SPM) (NT-MDT Ltd., Moscow, Russia). Silicon cantilevers with spring constant of 5.5 N/m and typical resonance frequency of 290 kHz were utilized.

3. Results and discussion

Fig. 1 shows X-ray diffraction patterns of the solid samples drawn off the reaction mixture at $t_c = 0$ (a), $t_c =$ 10 min (b), $t_c = 30$ min (c), $t_c = 90$ min (d) and $t_c = 240$ min (e). The X-ray diffraction patterns a, b and c do not have sharp maxima characteristic of crystalline phase (zeolite), but only a broad "maximum" characteristic of true amorphous precipitated aluminosilicates [26,47,48], having the molar oxide composition: $Na_2O \cdot Al_2O_3 \cdot 2.576\text{-}SiO_2 \cdot 2.28H_2O$. The amorphous nature of the samples drawn off the reaction mixture at $t_c = 0$ is also revealed by comparison of its FTIR spectrum (FTIR spectrum a in Fig. 2) with the FTIR spectrum of fully crystalline zeolite A (final product of crystallization as identified by the X-ray diffraction pattern e in Fig. 1 and FTIR spectrum b in Fig. 2) [49].

Since IR vibrations of zeolite skeleton are intense for agglomerates of even a few unit cells [50], the absence of the intense band at 556 cm^{-1} (assigned to external vibrations related to D-4 rings in zeolite A framework; see FTIR spectrum b in Fig. 2), reveals that the specific profiles of the X-ray spectra a, b and c in Fig. 1 are caused by the true amorphous nature of the corresponding samples, and not by the low amount of the crystalline phase and/or lowering of crystal size below X-ray detection limit [19,39]. However, the weak broad band in the frequency range between

Please cite this article in press as: C. Kosanović et al., Micropor. Mesopor. Mater. (2007), doi:10.1016/j.micromeso.2007.06.007

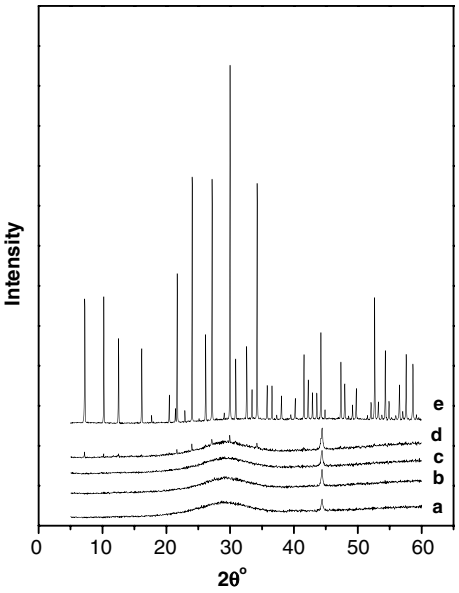

Fig. 1. X-ray diffraction patterns of freshly precipitated amorphous aluminosilicate precursor (gel; $t_c = 0$) (pattern a) and of the solid phases drawn off the reaction mixture (hydrogel) during its hydrothermal treatment at 80 °C for 10 min (pattern b), 30 min (pattern c), 90 min (pattern d) and 240 min (pattern e).

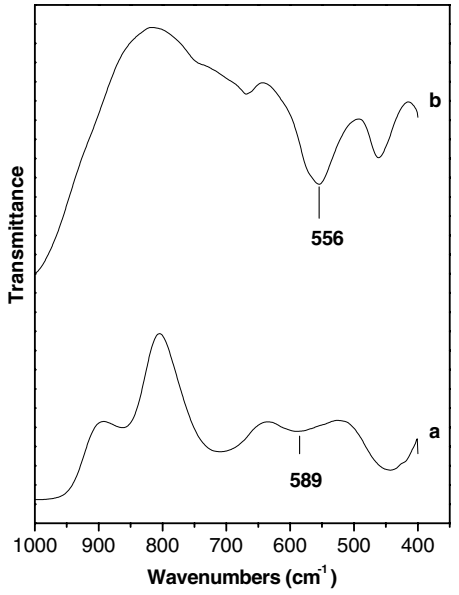

Fig. 2. FTIR spectra of freshly precipitated X-ray amorphous aluminosilicate precursor (gel; $t_c = 0$) (spectrum a) and of the solid sample drawn off the reaction mixture after its hydrothermal treatment at 80 °C for $t_c = 240$ min (spectrum b).

510 cm^{-1} and 650 cm^{-1} with a minimum at 589 cm^{-1} in the FTIR spectrum a in Fig. 2 is probably caused by the presence of the nano-sized, partially crystalline (''quasi-crystalline'') particles, that potentially be zeolite nuclei [19,26], which are also indicated by other experimental methods [15,16,18,19,22,37–40]. Prolonged heating of hydrogel causes a gradual transformation of amorphous to crystalline phase, as shown in X-ray diffraction pattern d in Fig. 1, and formation of pure zeolite A for $t_c = 240$ min (X-ray diffraction pattern e in Fig. 1 and FTIR spectrum b in Fig. 2).

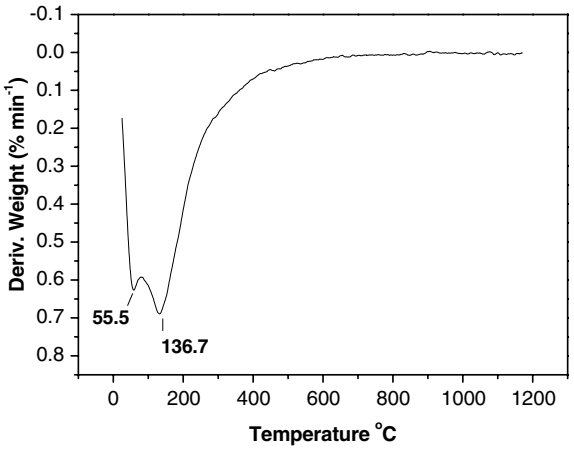

Fig. 3. DTG curve of freshly precipitated X-ray amorphous aluminosilicate precursor (gel; $t_c = 0$).

In addition, the presence of the endothermic minimum at $T \approx 137$ °C in the DTG curve of the X-ray amorphous aluminosilicate precursor (gel, Fig. 3), which position is close to the position of the endothermic minimum in the DTG curve of zeolite A (120–170 °C) [18,19] also indicates the presence of long-range ordered aluminosilicate (partially or ''quasi-crystalline'') phase in the gel matrix [18,19].

Fig. 4A–C shows HRTEM images of the X-ray amorphous aluminosilicate precursor (gel). The sample consists of unit globular features, 20–50 nm in size. Neither long-range ordered aluminosilicate phase in the form of the particles of partly or ''quasi-crystalline'' phase [16,40] nor small nano-sized zeolite crystals [15,20] can be observed in the gel matrix, even at very high magnification (Fig. 4C). The reason is probably the same as already indicated by Valtchev and Bozhilov [20,21], namely that ''HRTEM imaging did not bring information about the exact location of the zeolite nuclei, which most probably was due to the fact that they are extremely unstable and collapse under the high intensity electron beam necessary for HRTEM imaging or they did not produce detectable contrast in TEM because they were fully embedded in the amorphous gel''. However, knowing that electron diffraction of zeolites is intense for agglomerates of even a few unit cells [39], the appearance of the few faint diffraction circles of the electron diffraction pattern of gel (see Fig. 5) undoubtedly indicates that the X-ray amorphous solid contains particles of partially or ''quasi-crystalline'' phase having a size below the X-ray diffraction detection limit, but above the electron diffraction detection limit [19,39].

Since atomic force microscopy enabled the detailed observation of a nanometer-sized events, the gel is additionally analyzed by atomic force microscopy.

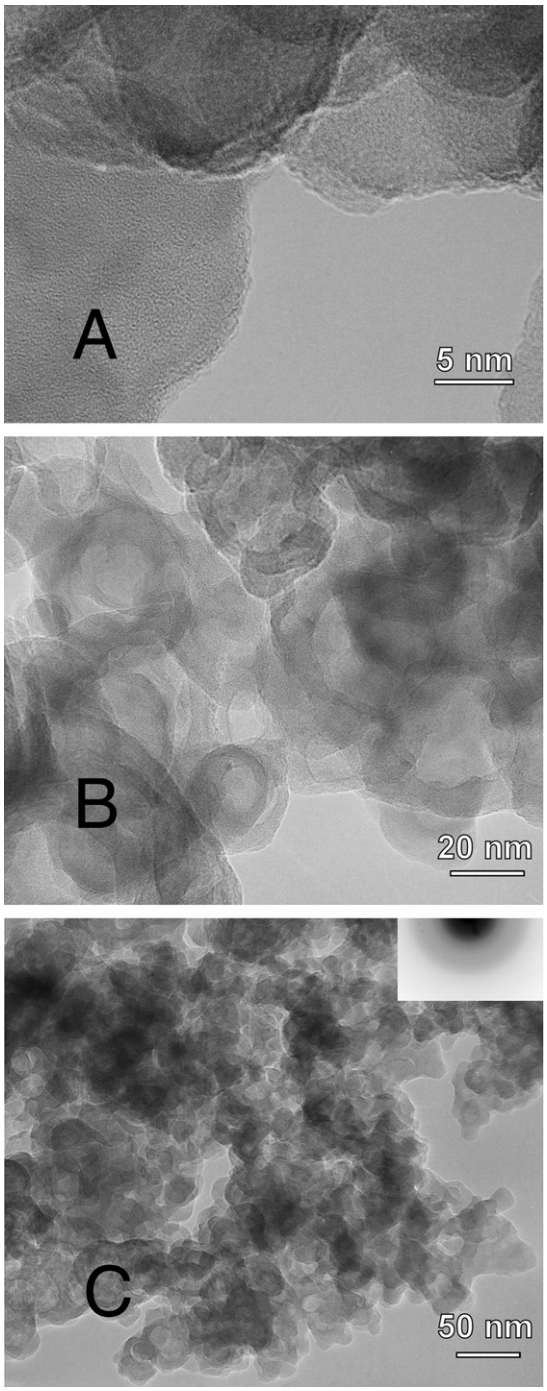

Fig. 4. HRTEM micrographs (A, B and C) of freshly precipitated X-ray amorphous aluminosilicate precursor (gel; $t_c = 0$). The figures A, B and C correspond to different magnification M: $M(B) = 4 \times M(A)$ and $M(C) = 10 \times M(A)$.

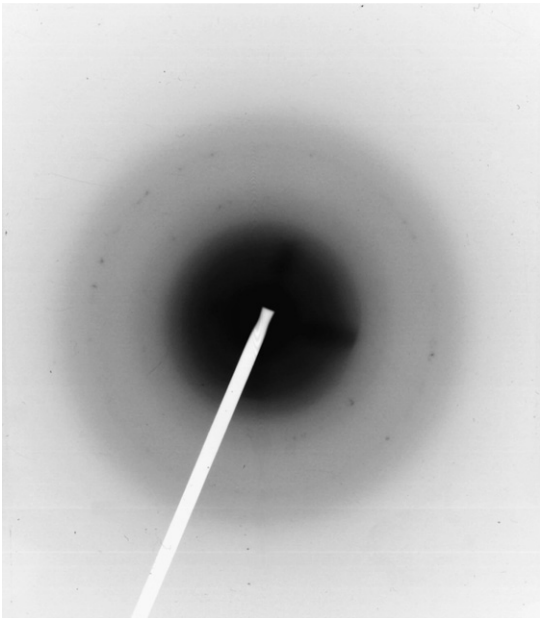

Fig. 5. Electron-diffraction pattern of freshly precipitated X-ray amorphous aluminosilicate precursor (gel; $t_c = 0$).

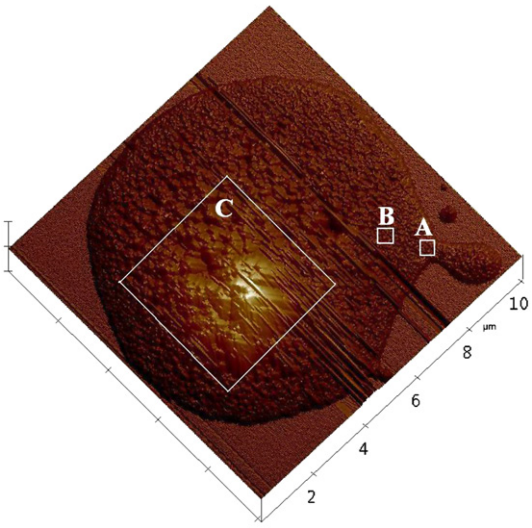

Fig. 6. AFM image of the X-ray amorphous aluminosilicate precursor (gel; $t_c = 0$). Surface plot of height data taken in contact mode, scan size 10×10 μm, the contrast covers the height variation from 0 to 1000 nm. Squares indicate the regions A, B and C shown at higher resolution in Fig. 7.

AFM image in Fig. 6 shows that X-ray amorphous aluminosilicate precursor (gel) contains three different types of nano-sized entities: (A) near-spheroidal-shaped particles (Figs. 6 and 7A), (B) ''transition'', probably partially crystalline, features (particles of ''quasi-crystalline'' phase [16,40]; see Figs. 6 and 7B) and (C) ''pyramidal-shape'' features which look like fully crystalline material (Figs. 6 and 7C). Since enlargement of the near-spheroidal-shaped particles does not result in an observing of some ''structural'' particularities (see Fig. 8), one can believe that just these particles represent the primary amorphous gel particles. A section-analysis (see Fig. 9) of the aggregate of the near-spheroidal-shaped particles (that also shown in Figs. 6, 7A and 8) shows that their cross-section diameters are in the range from 50 to 120 nm (mainly 80 nm) which is considerably higher than the cross-section diameters measured by HRTEM (10–50 nm; see Fig. 3). The difference

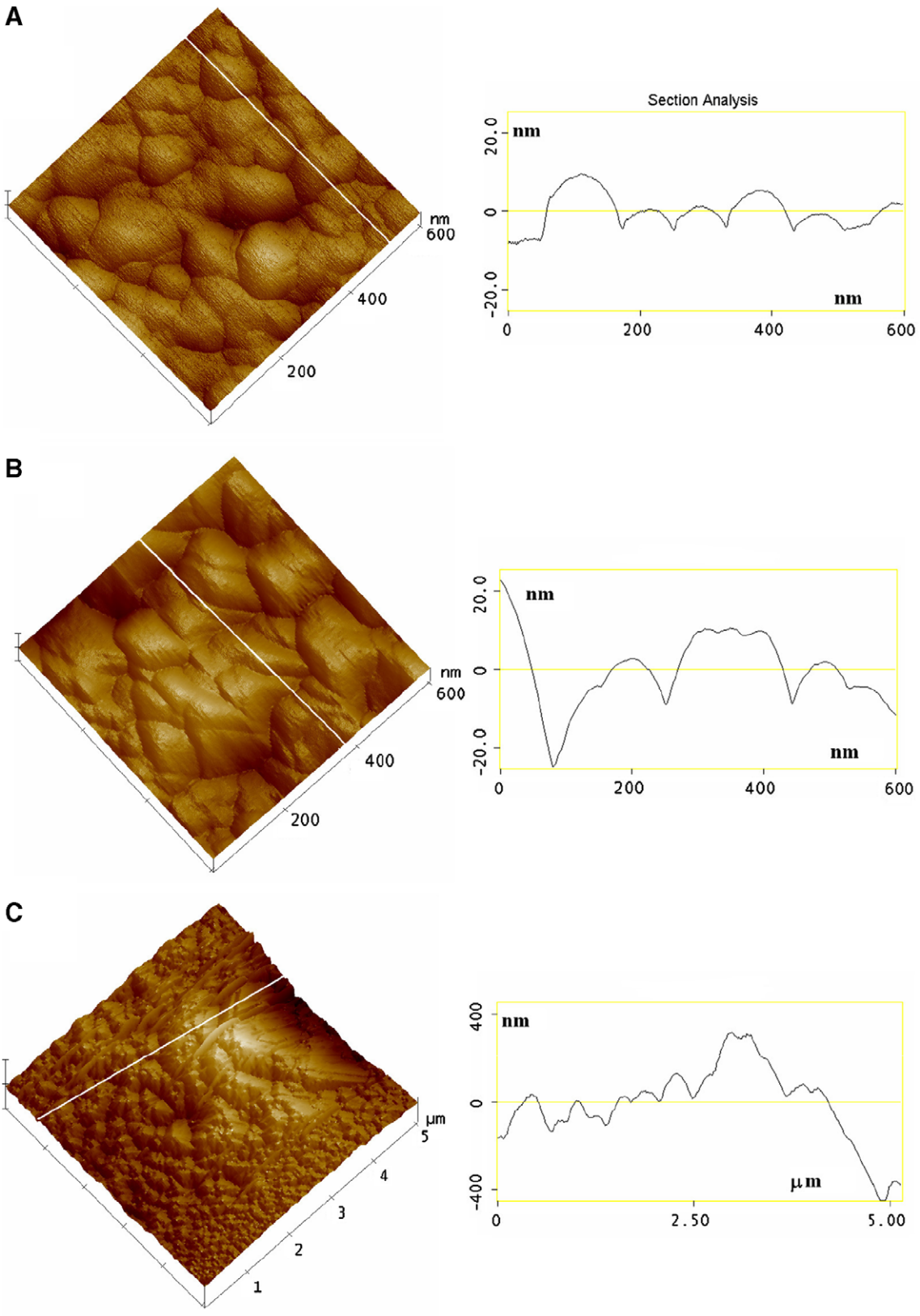

Fig. 7. AFM images of the regions A, B and C from Fig. 6 shown at a higher resolution together with corresponding topographic profiles along indicated lines (“section analyzes”). (A) region A, scan size 600 × 600 nm; (B) region B, scan size 600 × 600 nm; (C) region C, scan size 5 × 5 μm.

in the particle size measured by the two methods (HRTEM, AFM) was probably caused by different ways of sample preparation and measuring conditions; while HRTEM requires dehydrated samples and imaging under

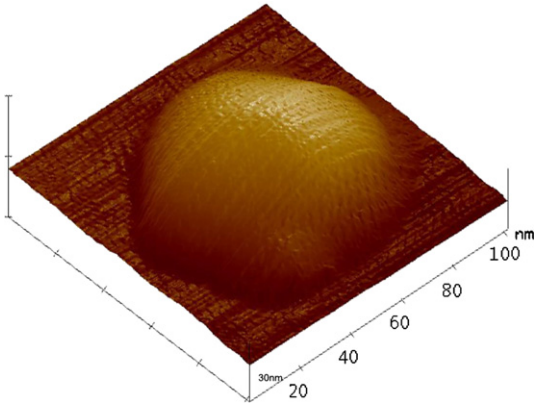

Fig. 8. AFM image of the disc-shaped particle (region A in Fig. 6) of X-ray amorphous aluminosilicate precursor (gel; $t_c = 0$); surface plot of height data taken in tapping mode, scan size 100×112 nm with vertical scale of 30 nm.

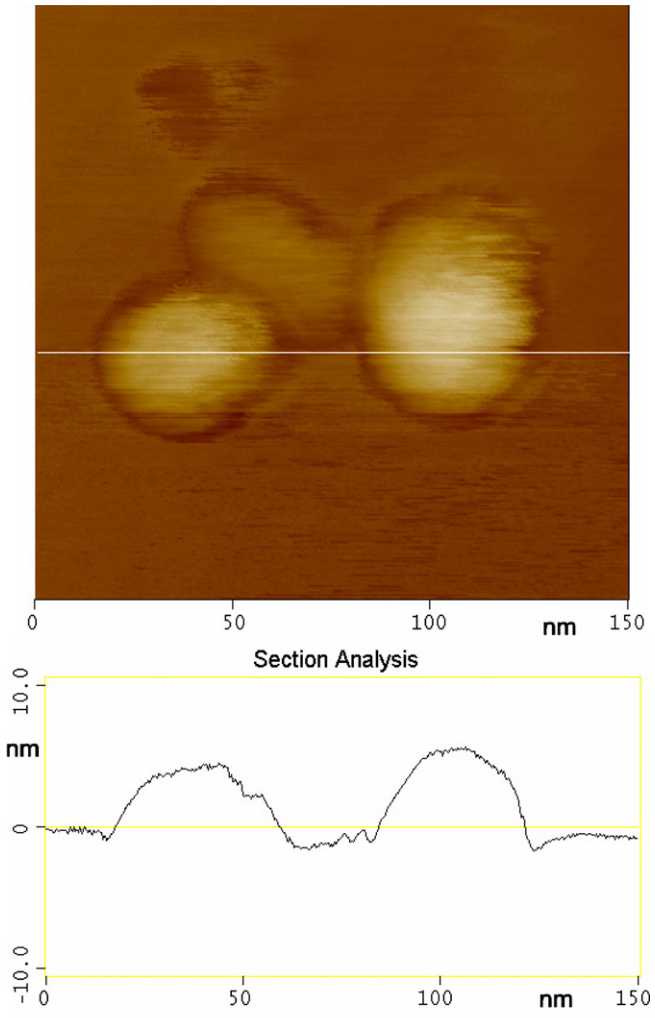

Fig. 9. AFM image of the disc-shaped particles of X-ray amorphous aluminosilicate precursor (gel; $t_c = 0$); top view of height data taken in tapping mode together with the topographic profiles along indicated line ("section analysis") of neighboring particles from region A in Fig. 6.

vacuum, the sample for AFM was suspended in water prior to the deposition on mica and imaging was kept under ambient conditions (50% humidity and normal pressure; see Section 2). This implies that original size of the moist "primary" particles (50–120 nm) is considerably reduced (to 10–50 nm) as the consequence of the shrinkage of the "primary" gel particles caused by their dehydration.

The section-analysis (see Fig. 9) of individual near-spheroidal-shaped particles (see also Fig. 8), clearly indicates that the "primary" particles are not spheres, but discs having a mean diameter of about 80 nm and mean height of about 15 nm. In addition, knowing that the characteristic height of the growing terraces of low-silica zeolites (zeolite A, faujasite) is about 1.2–1.4 nm which corresponds to the sizes of the unit cells of the mentioned zeolites [4–7,51], appearing of the vertical heights of 1.225 nm on some of the primary gel particles indicates the short-range ordering in the predominantly amorphous material. Hence, it seems that due to the high local supersaturation of constituents (Na, Si, Al) [12–15], the statistical conditions for the formation of not only amorphous phase, but also for the gradual formation of short- (Figs. 6, 7A, 8 and 9), medium-to-long (Figs. 6 and 7B) and long-range ordering (Figs. 6 and 7C), can be realized in the certain regions of gel, during its formation.

While the "pyramidal-shape" structures appear only in the form of aggregates in the freshly prepared gel (before thermal treatment of hydrogel; see Figs. 6 and 7C), the well developed single "pyramidal-shape" structures having a height of up to 220 nm can be found in the solid phase isolated from the reaction mixture after 30 min of heating at 80 °C (see Fig. 10A). The finding of the single "isolated", "pyramidal" shape structures at $t_c \geqslant 30$ min is in accordance with the principle of the autocatalytic nucleation [19,24–27,33,35]; namely that the less soluble, more structurally ordered entities "released" from the gel matrix dissolved during heating of hydrogel (crystallization). Hence, it is really to assume that just the small "pyramidal-shape" structures are nuclei of zeolite which start to grow after their release from the gel matrix, i.e., when they are in full contact with the liquid phase. On the other hand, one can expect that nuclei of zeolite A (which is the final product of crystallization) would be more or less of regular cubic shape, and not a "pyramidal" one with well developed triangular terraces; the vertical distances between two terraces are between 7 and 7.2 nm. Since the triangular terraces are characteristic for faujasites (zeolites X and Y) [4,7,51], it is realistic to assume that the "pyramidal-shape" structures (nuclei) shown in Fig. 10A have the crystal structure and chemical composition which are closer to faujasite than to zeolite A. Although strange at first sight, this can be readily explained by the fact that the ratio $y = SiO_2/Al_2O_3$ of amorphous aluminosilicate precursor (gel) is usually higher than 2 [52] ($y = 2.576$ in this case), which is more favorable for formation of faujasite ($y \geqslant 2.5$) [20] than zeolite A ($y = 2$) [21].

Please cite this article in press as: C. Kosanović et al., Micropor. Mesopor. Mater. (2007), doi:10.1016/j.micromeso.2007.06.007

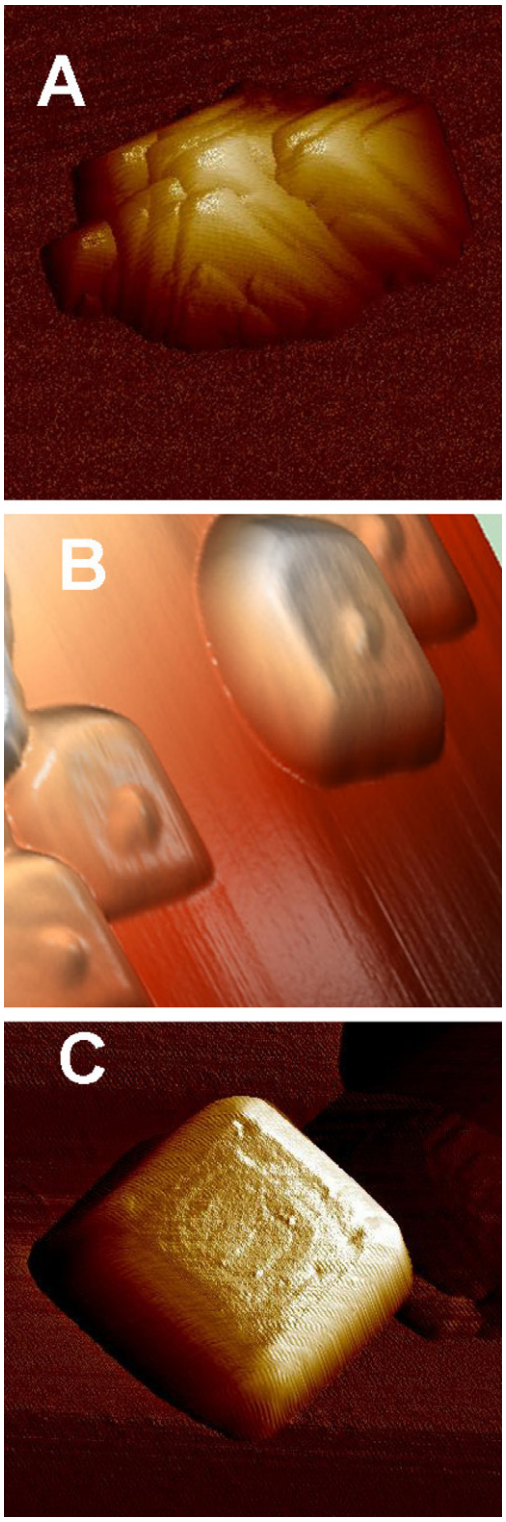

Fig. 10. AFM image of (A) the "pyramidal-shaped" particles contained in the solid phase drawn off the reaction mixture (hydrogel) after its hydrothermal treatment at 80 °C for 30 min (scan size: 1 × 1 μm; vertical scale: 250 nm), (B) near-cubic-shaped crystals contained in the solid phase drawn off the reaction mixture after its hydrothermal treatment at 80 °C for 90 min (scan size: 1 × 1 μm; vertical scale: 160 nm) and (C) typical cubic crystals of zeolite A contained in the solid phase drawn of the reaction mixture after its hydrothermal treatment at 80 °C for 240 min (scan size: 1.3 × 1.3 μm; vertical scale: 720 nm).

Knowing that vertical distance between growing triangle terraces of faujasite is about 1.43 nm, which corresponds to the height of unit cell of faujasite along ⟨1 1 1⟩ direction [4,7], it can be easily calculated that the thickness of each triangular terrace, shown in Fig 10A, corresponds to five unit cells of faujasite, i.e., (mean height of triangular terrace)/(height of unit cell of faujasite) = 7.1/1.43 = 4.965 5. However, the meaning of this data is not quite clear at present.

Fig. 10B shows the AFM image(s) of the crystals and/or crystal aggregates formed at $t_c = 90$ min. The near-cubic-shape of the formed crystals indicates that growth of the "pyramidal-shape" nuclei having faujasite structure results in the formation of zeolite A (initial step of faujasite overgrowth by zeolite A), as it indicated by the appearing of the X-ray diffraction peaks of zeolite A in the X-ray diffraction pattern of the solid phase drawn off the reaction mixture at $t_c = 90$ min (X-ray diffraction pattern d in Fig. 1): Note that the solid phase consists of mainly X-ray amorphous aluminosilicate (gel), so that the isolated crystals shown in Fig. 10B represent rarely appearing features in predominantly amorphous environment. Since there are numerous indications that the type of crystallized zeolite does not depend on the "structure" of nuclei, but on the concentrations of aluminum and silicon in the liquid phase of the crystallizing system (reaction mixture) [23,24,26,53], crystallization of zeolite A even on the nuclei of faujasite structure, was expected. Namely, as the ratio SiO_2/Al_2O_3 in the starting hydrogel is 2.15, and the ratio SiO_2/Al_2O_3 in the gel is 2.576, the liquid phase of the crystallizing system is "enriched" in aluminum, which is favorable for crystallization of zeolite A [53], which is also evidenced by the X-ray diffraction pattern e in Fig. 1 as well as by typical cubic-shape crystals of zeolite A shown in Fig. 10C.

4. Conclusion

Analysis of the precipitated sodium aluminosilicate precursor (gel) by different methods (FTIR, DTG, electron diffraction), has shown that predominantly true amorphous phase of the gel contains small proportions of partially crystalline ("quasi-crystalline") or even fully crystalline phase. This finding is also confirmed by AFM. Namely three different entities can be observed in the AFM images of the freshly prepared gel; aggregate of disc-shaped particles (having the mean diameter of about 80 nm and mean height of about 15 nm), "transition", probably partially crystalline, features (particles of "quasi-crystalline" phase) and aggregates of "pyramidal-shape" features which look like fully crystalline material. Since enlargement of the disc-shaped particles does not result in an observing of some "structural" particularities, it is concluded that just these particles represent the primary amorphous gel particles. Observation of isolated "pyramidal-shaped" particles in the AFM images of the

X-ray amorphous solid phase extracted from hydrogel after their heating at 80 °C for 30 min, is in accordance with the principle of the autocatalytic nucleation, namely that the less soluble, more structurally ordered entities "released" from the gel matrix dissolved during heating of hydrogel. Hence, it can be concluded that just the "pyramidal-shaped" particles are zeolite nuclei. Specific "pyramidal" shape of the nuclei having triangle terraces with thickness of five unit cells of faujasite (zeolites X and Y), lead to the conclusion that the crystal structure of nuclei is closer to faujasite than zeolite A. This is explained by the fact that the silica to alumina ratio in the gel ($SiO_2/Al_2O_3 > 2$) favors formation of faujasite rather than zeolite A. On the other hand, since the type of zeolite to be formed does not depend on the structure of nuclei but on the concentrations of aluminum and silicon in the liquid phase of the crystallizing system, the formation of zeolite A (growth of zeolite A on the nuclei of faujasite) was expected from the used reaction mixture (hydrogel).

Acknowledgments

The authors thank the Ministry of Education, Science and Sport of the Republic of Croatia for its financial support. Also thanks to Dr. G. Huhn, Eotvos Lorand University, Department of Materials Physics, Pazmany P. s. 1/A, 1117 Budapest, Hungary, for monitoring AFM images.

References

[1] C.S. Cundy, P.A. Cox, Microporous Mesoporous Mater. 82 (2005) 1.
[2] R.M. Barrer, Hydrothermal Chemistry of Zeolites, Academic Press, London, 1982.
[3] B. Subotić, J. Bronić, in: S.M. Auerbach, K.A. Carrado, P.K. Dutta (Eds.), Handbook of Zeolite Science and Technology, Marcel Dekker Inc., New York, Basel, 2003, p. 129.
[4] M.W. Anderson, J.R. Agger, J.T. Thornton, N. Forsyth, Angew. Chem. Int. Ed. 35 (1996) 1210.
[5] J.R. Agger, N. Pervaiz, A.K. Cheetham, M.W. Anderson, J. Am. Chem. Soc. 120 (1998) 10754.
[6] S. Dumrul, S. Bazzana, J. Warzywoda, R.R. Biederman, A. Sacco Jr., Microporous Mesoporous Mater. 54 (2002) 79.
[7] T. Wakihara, T. Okubo, J. Chem. Eng. Jpn. 37 (2004) 669.
[8] R.W. Thompson, A. Dyer, Zeolites 5 (1985) 202.
[9] J.B. Nagy, P. Bodart, H. Collette, C. Fernandez, Z. Gabelica, A. Nastro, R. Aiello, J. Chem. Soc., Faraday Trans. 85 (1989) 2749.
[10] J. Warzywoda, R.D. Edelman, R.W. Thompson, Zeolites 11 (1991) 318.
[11] G. Golemme, A. Nastro, J.B. Nagy, B. Subotić, F. Crea, R. Aiello, Zeolites 11 (1991) 776.
[12] Y. Yan, S.R. Chaudhuri, A. Sarkar, Chem. Mater. 8 (1996) 473.
[13] L. Gora, K. Streletzky, R.W. Thompson, G.D.J. Phillies, Zeolites 18 (1997) 119.
[14] L. Gora, K. Streletzky, R.W. Thompson, G.D.J. Phillies, Zeolites 19 (1997) 98.
[15] S. Mintova, N.H. Olson, V. Valtchev, T. Bein, Science 283 (1999) 958.
[16] L.A. Bursill, J.M. Thomas, in: R. Sersale, C. Collela, R. Aiello (Eds.), Recent Progress Report and Discussions: Fifth International Zeolite Conference, Giannini, Naples, 1981, p. 25.
[17] O. Okamura, Y. Tsuruta, T. Satoh, Gypsum Lime 206 (1987) 23.
[18] R. Aiello, F. Crea, A. Nastro, B. Subotić, F. Testa, Zeolites 11 (1991) 767.
[19] B. Subotić, A.M. Tonejc, D. Bagović, T. Antonić, in: J. Weitkamp, H.G. Karge, H. Pfeifer, W. Hölderich (Eds.), Zeolites and Related Microporous Materials: State of the Art 1994, Studies in Surface Science and Catalysis, vol. 84A, Elsevier, Amsterdam, 1994, p. 259.
[20] V.P. Valtchev, K.N. Bozhilov, J. Phys. Chem. B 108 (2004) 15587.
[21] V.P. Valtchev, K.N. Bozhilov, J. Am. Chem. Soc. 127 (2005) 16171.
[22] S. Mintova, N.H. Olson, T. Bein, Angew. Chem. Int. Ed. 38 (1999) 3201.
[23] H. Kacirek, H. Lechert, J. Phys. Chem. 79 (1975) 1589.
[24] A. Katović, B. Subotić, I. Šmit, Lj.A. Despotović, Zeolites 9 (1989) 45.
[25] E. Narita, K. Sato, N. Yatabe, T. Okabe, Ind. Eng. Chem. Prod. Res. Dev. 24 (1985) 507.
[26] A. Katović, B. Subotić, I. Šmit, Lj.A. Despotović, M. Ćurić, in: M.L. Occelli, H.E. Robson (Eds.), Zeolite Synth., American Chemical Society Symposium Series, vol. 398, American Chemical Society, Washington, 1989, p. 124.
[27] B. Subotić, A. Graovac, in: B. Držaj, S. Hočevar, S. Pejovnik (Eds.), Zeolites: Synthesis, Structure, Technology and Application, Studies in Surface Science and Catalysis, vol. 24, Elsevier, Amsterdam, 1985, p. 199.
[28] J. Ciric, J. Colloid Interface Sci. 28 (1968) 315.
[29] X. Qinhua, B. Shulin, D. Jialu, Sci. Sinica 25 (1982) 349.
[30] G. Seo, Hwahak Konghak 23 (1985) 295.
[31] R.D. Edelman, D.V. Kudalkar, T. Ong, J. Warzywoda, R.W. Thompson, Zeolites 9 (1989) 496.
[32] H.V. Hu, W.H. Chen, T.Y. Lee, J. Cryst. Growth 108 (1991) 561.
[33] S. Gonthier, R.W. Thompson, in: J.C. Jansen, M. Stöcker, H.G. Karge, J. Weitkamp (Eds.), Advanced Zeolite Synthesis and Application, Studies in Surface Science and Catalysis, vol. 85, Elsevier, Amsterdam, 1994, p. 43.
[34] B. Subotić, T. Antonić, S. Bosnar, J. Bronić, M. Škreblin, in: I. Kiricsi, G. Pal-Borbely, J.B. Nagy, H.G. Karge (Eds.), Porous Materials in Environmentally Friendly Processes, Studies in Surface Science and Catalysis, vol. 125, Elsevier, Amsterdam, 1999, p. 157.
[35] C. Falamaki, M. Edrissi, M. Sohrabi, Zeolites 19 (1987) 2.
[36] G. Engelhardt, B. Fahlke, M. Mägi, E. Lippmaa, Zeolites 3 (1983) 292.
[37] Z. Gabelica, J.B. Nagy, G. Debras, E.G. Derouane, Acta Chim. Hung. 119 (1985) 275.
[38] M.D. Richards, C.G. Pope, J. Chem. Soc., Faraday Trans. 92 (1996) 317.
[39] Y. Tsuruta, T. Satoh, T. Yoshida, O. Okamura, S. Ueda, in: Y. Murakami, A. Iijma, J.W. Ward (Eds.), New Development in Zeolite Science, Kodansha Ltd., Tokyo, 1986, p. 1001.
[40] J.M. Thomas, L.A. Bursill, Angew. Chem. Int. Ed. Engl. 19 (1980) 754.
[41] S. Sugiyama, O. Matsuoka, H. Nozoye, J. Yu, G. Zhu, S. Qiu, O. Terasaki, Microporous Mesoporous Mater. 28 (1999) 1.
[42] M.W. Anderson, J.R. Agger, N. Hanif, O. Terasaki, Microporous Mesoporous Mater. 48 (2001) 1.
[43] J.R. Agger, N. Hanif, M.W. Anderson, Angew. Chem. Ind. Ed. 40 (2001) 4065.
[44] M.W. Anderson, Curr. Opin. Solid State Mater. Sci. 5 (2001) 407.
[45] M. Smaihi, O. Barida, V. Valtchev, Eur. J. Inorg. Chem. (2003) 4370.
[46] T. Wakihara, A. Sugiyama, T. Okubo, Microporous Mesoporous Mater. 70 (2004) 7.
[47] R.I. Walton, R.I. Smith, D. O'Hare, Microporous Mesoporous Mater. 48 (2001) 79.
[48] C.D. Cheng, A.T. Bell, Catal. Lett. 8 (1991) 305.
[49] E.M. Flanigen, H. Khatami, H.A. Szymanski, in: R.F. Gould (Ed.), Molecular Sieve Zeolites – I, Advances in Chemistry Series, vol. 101, American Chemical Society, Washington, DC, 1971, p. 201.
[50] P.A. Jacobs, E.G. Derouane, J. Weitkamp, J. Chem Soc., Chem. Commun. (1981) 591.
[51] J.R. Agger, M.W. Anderson, Stud. Surf. Sci. Catal. 142A (2002) 93.
[52] I. Krznarić, T. Antonić, B. Subotić, Microporous Mesoporous Mater. 20 (1998) 161.
[53] S. Bosnar, J. Bronić, I. Krznarić, B. Subotić, Croat. Chem. Acta 78 (2005) 1.